Imprintable, Bendable, and Shape-Conformable Polymer Electrolytes for Versatile-Shaped Lithium-Ion Batteries

Eun-Hye Kil, Keun-Ho Choi, Hyo-Jeong Ha, Sheng Xu, John A. Rogers, Mi Ri Kim, Young-Gi Lee, Kwang Man Kim, Kuk Young Cho, and Sang-Young Lee**

Rechargeable lithium-ion batteries, the most popular energy source for mobile electronic devices, are rapidly expanding their range of applications into fields such as electrical vehicles, grid energies, and flexible electronic devices.[1] This strong market demand stimulates the need for development of advanced lithium ion battery technologies capable of improving energy storage densities, cycle life, charge/discharge rates, and design flexibility.[2,3]

One strategy to address certain of these goals involves advanced structural design in the electrodes, along with associated new material development. For example, three dimensional (3D) electrodes can yield improvements in rate capability and capacity retention.[4–6] These advantages are further enhanced in high-capacity anode materials, such as silicon and tin, which undergo large changes in volume during charge/discharge cycling.[7,8] One challenge for 3D electrodes, particularly in integration of active components, arises from difficulties in securing conformal electrolytes that can also prevent electrical shorts between electrodes.[6] Although liquid electrolytes ensure excellent electrochemical performance and good physical contact with 3D electrodes, they suffer from potential leakage, leading to safety concerns. More importantly, liquid electrolytes limit choices in cell design due to their fluidic characteristics and the need for separator membranes in cell assembly. This situation motivates the development of self-supporting solid-state electrolytes that can conform to 3D electrodes and, at the same time, provide sufficient mechanical deformability for reliable use, especially for applications in flexible electronics and other demanding areas of envisioned use.

Among various solid-state electrolytes, gel polymer electrolytes (GPEs), which are generally composed of polymer matrix and liquid electrolyte, are widely used in lithium-ion batteries owing to their excellent ionic conductivity, low rates of safety failure, and mechanical flexibility.[9–11] In general, conventional GPEs are prepared using a predesigned frame via solution casting of liquid state mixtures (i.e., liquid electrolytes and polymers dissolved in organic solvents or liquid electrolytes/polymerizable monomers), followed by solvent evaporation or chemical cross-linking for solidification. The initial, liquid-state, mixtures for GPEs have limited dimensional stability before solidification due to their intrinsically fluidic characteristics, thereby restricting their facile application to complex-structured systems such as 3D batteries.

To the best of our knowledge, there are no polymer electrolytes that are both shape-conformable to 3D electrodes and mechanically flexible without impairing their electrochemical performance. Moreover, it is still challenging to secure dimensional stability (as a solid form) of polymer electrolytes during electrolyte preparation and cell assembly process.[6,12]

In the following, we demonstrate a facile and scalable approach to the fabrication of highly ion-conductive and bendable polymer electrolytes that can be also conformable to 3D micropatterned architectures of electrodes over large areas. These polymer electrolytes can also be directly writable or printable onto substrates of interest (including electrodes with complex geometries) due to well-tuned rheological characteristics. The materials are a kind of composite gel polymer electrolyte (hereinafter, referred to as "c-GPE"), composed of a UV (ultraviolet)-cured ethoxylated trimethylolpropane triacrylate (ETPTA) polymer matrix, high-boiling point liquid electrolyte (1M $LiPF_6$ in ethylene carbonate (EC)/propylene carbonate (PC) = 1/1 (v/v)), and alumina (Al_2O_3) nanoparticles (**Figure 1**a). The ETPTA monomer, which contains trivalent vinyl groups that participate in UV-crosslinking,[13,14] serves as a mechanical framework (after UV-curing). The chemical structure of the ETPTA, along with 2-hydroxy-2-methyl-1-phenyl-1-propanon (HMPP, a photo-initiator), appears in Figure S1 in ESI. The Al_2O_3 nanoparticles are incorporated as a functional filler to control the rheological properties of the electrolyte mixture and enable direct printing on a substrate such as an electrode.

As a control sample, an electrolyte mixture (hereinafter, referred as "F-solution") comprised of the ETPTA monomer and liquid electrolyte without Al_2O_3 nanoparticles, was also

E.-H. Kil, K.-H. Choi, H.-J. Ha
Department of Chemical Engineering
Kangwon National University
Kangwondaehak-gil, Chuncheon,
Kangwon, 200-701, Korea
Dr. S. Xu, Prof. J. A. Rogers
Department of Materials Science and Engineering
University of Illinois at Urbana-Champaign; Goodwin St., Urbana, IL 61822, USA
M. R. Kim, Prof. K. Y. Cho
Division of Advanced Materials Engineering
Kongju National University
1223-24, Cheonan-daero, Cheonan, Chungnam, 331-717, Korea
E-mail: kycho@kongju.ac.kr
Dr. Y.-G. Lee, Dr. K. M. Kim
Power Control Device Research Team
Electronics and Telecommunications Research Institute (ETRI)
218, Gajeongno, Yuseong-gu, Daejeon, 305-700, Korea
Prof. S.-Y. Lee
Interdisciplinary School of Green Energy
Ulsan National Institute of Science and Technology (UNIST)
Ulsan, 689-798, Korea
E-mail: sangyounglee87@gmail.com

DOI: 10.1002/adma.201204182

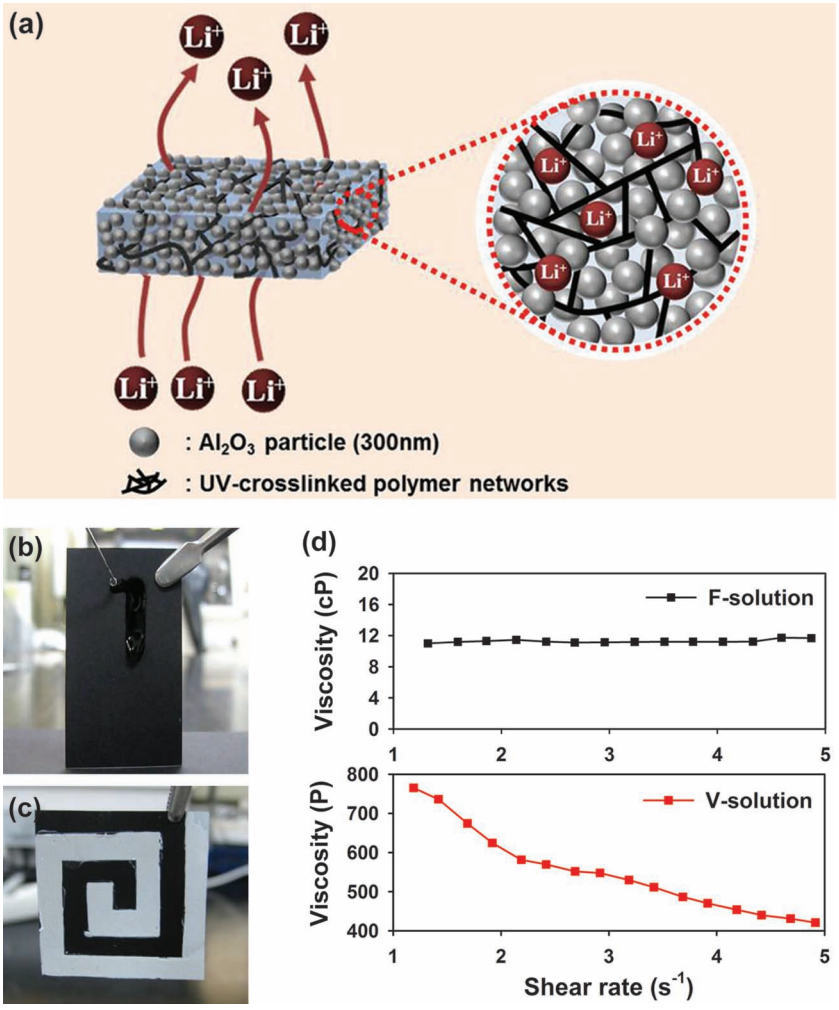

Figure 1. a) Conceptual illustration of an imprintable, flexible, shape-conformable c-GPE. b) Dripping characteristic of a liquid electrolyte that does not incorporate Al_2O_3 nanoparticles (designated as F-solution). c) Non-dripping behavior of UV-curable electrolyte mixture before UV-crosslinking reaction (designated as V-solution). d) Comparison of viscosity (as a function of shear rate) between the F- and V-solution.

cast onto an $LiCoO_2$ cathode. Due to its fluidic character, the F-solution flows easily when it is vertically tilted (Figure 1b). By contrast, an otherwise similar solution with Al_2O_3 nanoparticles (hereinafter, referred as "V-solution") is highly viscous and undergoes limited flow even before UV crosslinking (Figure 1c). Viscosity measurements reveal that the F-solution exhibits traditional Newtonian behavior, yielding a viscosity of 11 cP. The V-solution, on the other hand, shows a non-Newtonian response, (i.e., typical shear-thinning behavior), wherein the viscosity increases by 4 orders of magnitude as compared to the F-solution (Figure 1d). This unique rheological feature of the V-solution can facilitate its application in writable or printable electrolyte systems.

It should be noted that the rheological behavior of the V-solution depends strongly on composition ratio and dispersion state of the Al_2O_3 nanoparticles. Here, the Al_2O_3 content was varied between 33% and 80%, as determined by the amount of Al_2O_3 in total weight (= Al_2O_3 + ETPTA + liquid electrolyte) (See Figure S2 in ESI). Among the various compositions, an Al_2O_3 content of 66% was found to exhibit optimal rheological properties, for printing and comforming to complex-structured substrates.

Direct UV-assisted nanoimprint lithography (UV-NIL)[15–18] was exploited to construct 3D shape-comformable polymer electrolytes from the rheologically tuned V-solution. The UV-IL technique is a well known, versatile patterning technology for production of diverse micro- and nanostructures for microelectronics, optoelectronic devices, and high-density magnetic data storage. Here, we used PDMS stamps for UV-NIL, featuring a maze-like structure with a repeating surface grating (wall thickness and height were 10 μm, respectively) in 1.5 cm × 1.5 cm dimensions. We also explored silicon anode pillars on a rigid silicon wafer as columnar structure[6,19], of a type that is prefered for 3D electrodes designed to accomodate severe volume change during charge-discharge cycle. These two structures were used to investigate not only the applicability of polymer electrolyte on flexible and rigid substrates but also replication of round and angular patterns. PDMS stamps were formed using the casting and curing procedures of soft lithography with a master fabricated by exposure (365 nm UV mask-aligner; Karl-Suss) of photoresist SU-8 (Micro Chem) on a silicon wafer. Pressing such stamps against cast layers of V-solutions followed by UV exposure through the stamps yielded solid replicas while in contact (**Figure 2**a). A SEM image of a molded c-GPE with maze patterns demonstrates the high fidelity that can be achieved in this process, where the structures show well-defined vertical edge profiles and high mechanical stability (Figure 2b). A high-magnification, cross sectional SEM image shows that the Al_2O_3 nanoparticles are uniformly dispersed through the c-GPE (see Figure S3 in ESI).

The mechanical bendability of the c-GPE as a self-standing film (thickness ~ 150 μm) was quantitatively measured using a bending test (under longituidinal strain ranged from 10 to 30 mm, strain rate = 10 mm·min^{-1}). The c-GPE offers strong resistance to mechanical breakage upon appreciable bending (bending radius ~ 0.5 cm), even at a low concentration of polymer matrix (i.e., ETPTA/liquid electrolyte = 15/85 w/w). Also, the c-GPE retains dimensional stability until the 29th bending cycle. (Fracture occurs upon additional cycles, as in Figure S4 in ESI). The c-GPE was also mechanically stable under the twisting (bending radius ~ 0.35 cm) (Figure 2c) deformations. Moreover, the maze patterns do not distort even after being subjected to five cycles of bending stress (bending radius ~ 0.5 cm) (see Figure S5 in ESI), which reflects the excellent structural stability of the c-GPE.

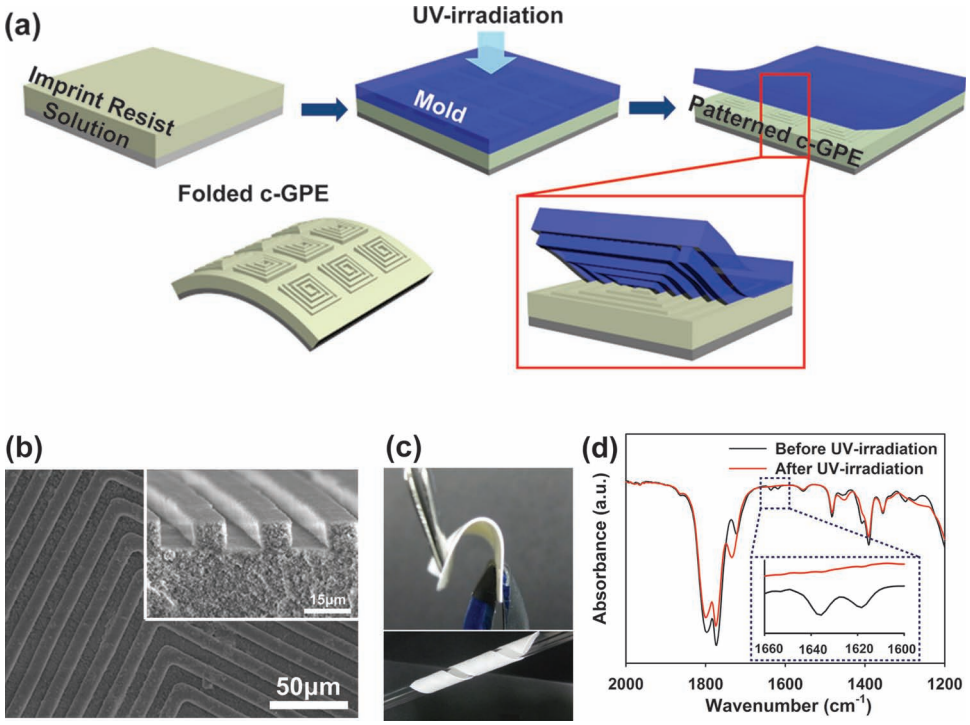

Figure 2. a) Steps for fabricating an imprintable, bendable, and shape-conformable polymer electrolyte (c-GPE) via direct UV-assisted nanoimprint lithography (UV-NIL) b) A SEM photograph (surface) of a c-GPE with a maze-pattern (an inset is a cross-sectional image). c) Photographs demonstrating highly-bendable and twistable features of c-GPE. d) FT-IR spectra depicting acrylic C = C double bonds of V-solution (before UV-irradiation) and c-GPE (after UV-irradiation).

The FT-IR measurements before and after UV-irradiation show that the characteristic peaks assgined to acrylic C = C bonds (1610 ~ 1625 cm^{-1})[13,14] disappear (Figure 2d), which verifies that the crosslinking reaction is successfully completed in the c-GPE. This process was further confirmed by estimating the gel content of c-GPE, after solvent (dimethyl carbonate followed by acetone) extraction to remove the incorporated liquid electrolytes and any unreacted monomers.[20] Over 99% by weight remained relative to the initial weight of UV curable monomer. This result verifies that the UV-curing reaction of ETPTA monomer in the c-GPE was nearly complete. The solid electrolyte characteristics (electrochemical stability, ionic conductivity, and cell performance) of the c-GPE are examined. Linear sweep voltammograms indicate that no significant decomposition of any components in the c-GPE takes place below 4.5 V vs. Li/Li^+. This high anodic stability suggests potential for application to high-voltage lithium-ion batteries (**Figure 3**a). Figure 3a shows that the ionic conductivity of the c-GPE is more than 10^{-3} S cm^{-1} at room temperature, with values that increase with temperature. Another advantageous feature of the c-GPE is that no weight loss is observed below temperature of 100 °C, as observed from the TGA result due to the presence of high-boiling point liquid electrolyte (i.e., 1M $LiPF_6$ in EC/PC) (Figure 3b).

Cycling performance of the cell ($LiCoO_2$ cathode/c-GPE/lithium metal anode) was examined using a flat c-GPE film, where the cell was cycled between 3.0 and 4.2 V at a constant charge/discharge current density (= 0.5 C/0.5 C). The cell exhibits highly stable charge/discharge profiles up to the 50th cycle (Figure 3c). In addition, the couloumb efficiency is ~97%, thereby contributing to the negligible capacity loss during cycling (Figure 3d).

To explore the feasibility of applying the c-GPE to 3D-electrodes, cells were prepared using silicon anodes that are patterned into arrays of columns supported by similarly structured copper on a silicon wafer. The fabrication involved sputter deposition of silicon to a thickness of ~40 nm onto the copper in pillars with heights of 18 μm,[21] where the electrode area is 0.9 cm × 0.9 cm. The electrode was incorporated into a cell that employs lithium metal as the counter electrode and c-GPE as the solid electrolyte (see Figure S6 in ESI). As shown in **Figure 4**, an inverse replica of the 3D silicon structure is successfully formed in the c-GPE, allowing good contact with the anode. Analysis of the SEM images (Figure 4c) shows that the imprinted c-GPE has a height (18 μm) and radius (~153 μm), well matched with the dimension of the 3D silicon anode.

Figure 4a shows the cycling performance of the cell (Si anode/c-GPE/Li metal) using inversely-replicated c-GPE as an electrolyte, where the cell was cycled between 0.01 and 1.5 V at a constant charge/discharge current density (= 0.5 C/0.5 C). The cell shows capacity loss due to SEI (solid electrolyte interphase) layer formation at the first cycle and gradual capacity decay afterwards. This charge/discharge behavior of the cell is similar to the previously reported results for 3D Si anodes.[22] From a calculation based on the 40 nm thickness silicon, the initial charge (i.e., lithiation of silicon anode) capacity is found

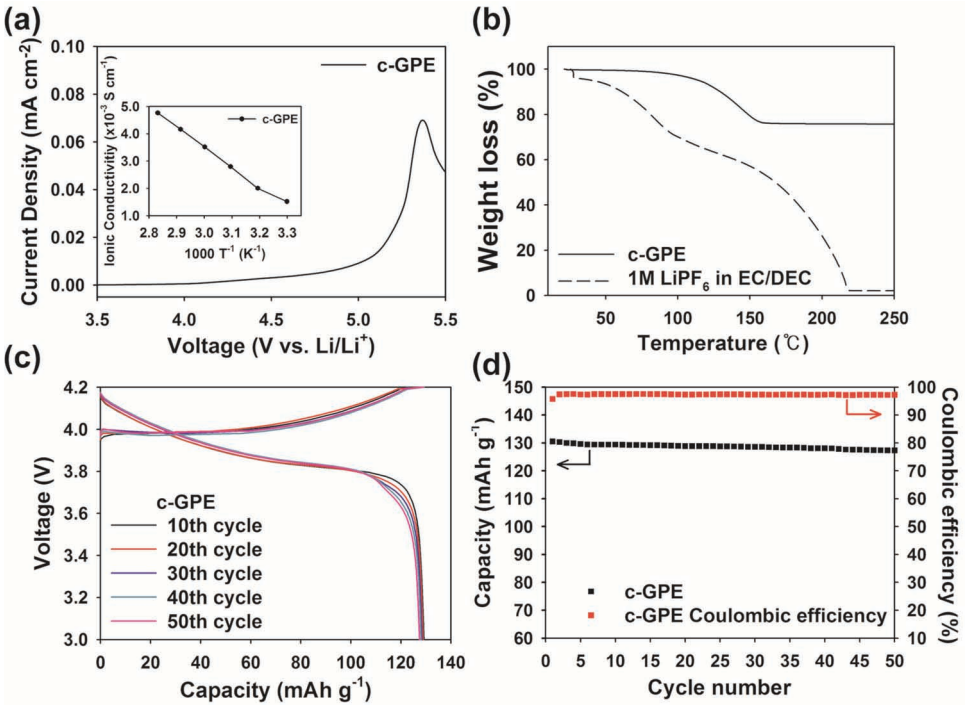

Figure 3. a) Electrochemical stability window for a c-GPE (an inset shows temperature-dependent ionic conductivity of c-GPE). b) TGA profiles showing difference in thermal stability compared to a conventional carbonate-based liquid electrolyte (1M $LiPF_6$ in EC/DEC = 1/1 v/v) and c-GPE. c) Charge/discharge profiles of a cell (lithium metal/flat-shaped c-GPE/$LiCoO_2$ cathode) as a function of cycle number (at a constant charge/discharge current density = 0.5 C/0.5 C under a voltage range of 3.0–4.2 V). d) Cycling performance (= capacity retention with cycling and coulombic efficiency of a cell, lithium metal/flat-shaped c-GPE/$LiCoO_2$ cathode).

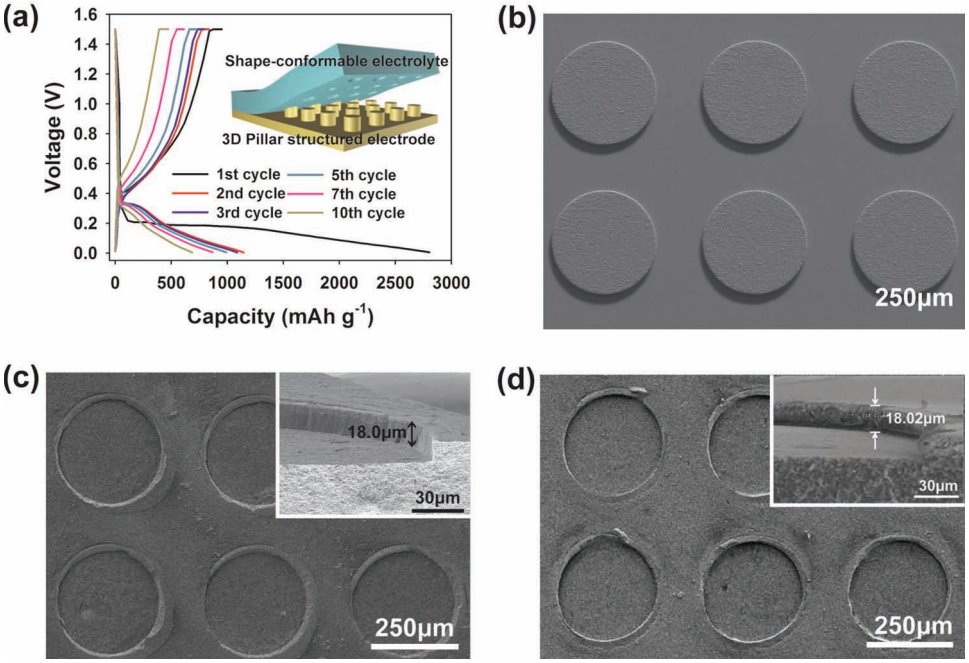

Figure 4. a) Charge/discharge profiles of a cell comprising a 3D Si anode/c-GPE/lithium metal as a function of cycle number (at a constant charge/discharge current density = 0.5 C/0.5 C under a voltage range of 0.01–1.5 V). b) A SEM photograph of a 3D pillar (height = 18 μm, radius = 153 μm) structured current collector. c) A SEM photograph (surface) of inversely-replicated c-GPE (i.e., after being detached from the 3D pillar structured Si anode), where the inset is a cross-sectional image. d) A SEM photograph (surface) of an inversely-replicated c-GPE disassembled from a cell after the 10^{th} cycle of operation (the inset is a cross-sectional image).

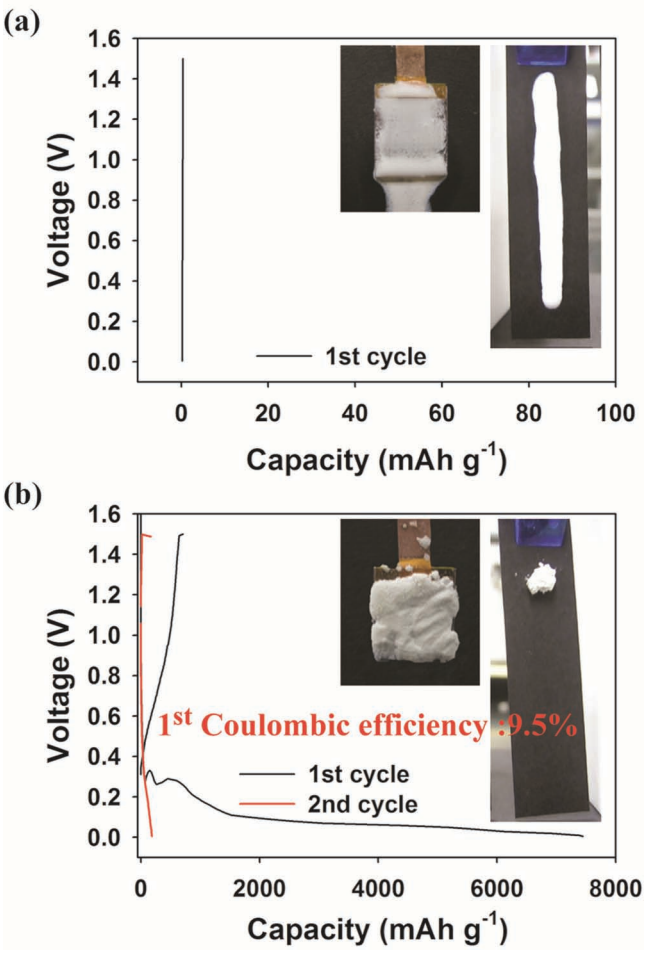

Figure 5. Charge/discharge profiles of a cell comprising 3D Si anode/non-optimized c-GPE/lithium metal as a function of cycle number (at a constant charge/discharge current density = 0.5 C/0.5 C): (a) Al_2O_3 content = 33%; (b) Al_2O_3 content = 80%.

to be 2680 mAh g^{-1}. Although the capacity retention with cycling is not ideal, because the 3D-structured cells are not optimized, the overall cycling performance is promising compared to that of c-GPE with non-optimized Al_2O_3 content. Moreover, Figure 4d shows that the inversely-replicated structure of the c-GPE is almost unchanged, even after the 10th cycle, compared to the initial shape (Figure 4c). This result demonstrates dimensional stability in the imprinted c-GPE and verifies the successful application of the shape-conformable c-GPE to the 3D-structured cells. It also suggests that the good cycling performance in the optimized c-GPE formulation results from its outstanding imprintability, shape conformability, flexibility, and electrochemical performance. These attributes can facilitate the development of 3D-structured battery systems.

Figure 5 shows that Al_2O_3 content of 33% (or 80%) leads to unsuccessful integration on 3D Si anodes due to non-optimized rheological properties, consistent with the previous result (Figure S2). It should be noted that the structure of the imprinted c-GPEs has a significant influence on the cell performance. For instance, c-GPE with Al_2O_3 content of 33%, where the c-GPE exhibits highly fluidic characteristic, most of the 3D Si anode remains uncoated. As a result, no meaningful charge/discharge reaction is obtained, likely due to internal short-circuit between the anode and cathode. For c-GPE with Al_2O_3 content of 80%, the Al_2O_3 nanoparticles agglomerate, and the c-GPE does not completely cover the 3D Si anode. The mechanical compliance diminishes, and large-sized pinholes and cracks appear. Due to this non-uniform morphology of the imprinted c-GPE, the cell assembled with the c-GPE does not provide normal charge/discharge behavior. More specifically, excessively large charge capacity and very low coulombic efficiency (~ 9%) at the 1st cycle are observed. The cell in this case might be partially internally short-circuited due to the poorly-imprinted c-GPE on the 3D Si anode.

In summary, we successfully fabricated highly ion-conductive, bendable polymer electrolytes that are also conformable to 3D micropatterned architectures of electrodes over large areas. More notably, the polymer electrolytes can be directly writable or printable onto complex, contoured substrates, owing to the structural uniqueness and well-tuned rheological characteristics. A persistent challenge in the development of 3D-structured or flexible batteries is in the maintenance of good contact between polymer electrolytes and electrodes, to facilitate electrochemical reaction at the interface. In this respect, the polymer electrolytes introduced here can be important.

Experimental Section

Fabrication of bendable polymer electrolytes with maze-imprinted micropatterns: A UV-curable electrolyte mixture was prepared by mixing liquid electrolyte (1 M $LiPF_6$ in EC/PC = 1/1 v/v, Soulbrain), ETPTA (Mw = 428, trivalent acrylate monomer), 2-hydroxy-2-methyl-1-phenyl-1-propanon (HMPP, photo-initiator), and vacuum-dried Al_2O_3 nanoparticles (average particle size = 300 nm, Sumitomo Chemical). The weight-based composition ratio of the (ETPTA/liquid electrolyte = 15/85 w/w)/Al_2O_3 = 34/66 w/w, wherein the concentration of HMPP was fixed at 1.0 wt% of ETPTA. The solution was then subjected to vigorous mixing via bead-milling for 0.5 h, to yield uniform dispersions of Al_2O_3 nanoparticles. Meanwhile, PDMS stamps with maze-patterns were prepared from a commercially available liquid prepolymer mixture of a silicon elastomer base and curing agent (Sylgard 184, Dow Corning). The mixture of elastomer base and curing agent (= 91/9 w/w) was vigorously stirred at 350 rpm for 40 min. Any bubbles generated during mixing were removed by repeatedly evacuating and purging the mixtures in a vacuum oven. A PDMS stamp with the maze-patterns was obtained by thermal curing of the prepolymer mixture on a photoresist master at 80 °C for 5 h. The cured PDMS was then peeled off from the master.

The aforementioned UV-curable electrolyte mixture (i.e., imprint resist solution) was cast onto a poly(ethylene terephthalate) (PET) sheet and then was mechanically imprinted with a maze-patterned PDMS stamp in an argon-filled glove box. The imprint resist solution was then exposed to UV irradiation for 20 sec through the transparent PDMS stamp to solidify the replica while in contact with the stamp. After the PDMS stamp was peeled off, self-standing and bendable composite gel polymer electrolytes (c-GPEs) in the inverse replica geometry of the maze patterns were obtained. The thickness of the c-GPEs was ~150 μm. The UV curing was conducted using a Hg UV lamp (100 W, Lichtzen), with a radiation peak intensity of approximately 2000 mWcm^{-2} at the surface of the samples.

Characterization of structured polymer electrolytes for versatile-shaped batteries: The maze-imprinted micropatterns of the c-GPE were examined with a field emission scanning electron microscope (FE-SEM, S-4300, Hitachi) and an optical microscope (OM, BX41, Olympus). The viscosity of the UV-curable electrolyte mixture was measured with a viscometer (RVDV-II, Brookfield). The UV curing reaction of the c-GPE was

elucidated with a FT-IR spectrometer (FT-3000, Excalibur) with a spectral resolution of 4 cm^{-1}. The electrochemical stability window of the c-GPE was estimated with linear sweep voltammetry performed on a working electrode of stainless-steel and a counter and reference electrode of Li metal at a scan rate of 1.0 mV s^{-1}. The ionic conductivity of the c-GPE was estimated with an impedance analyzer (VSP classic, Bio-Logic) over a frequency range of 1 to 10^6 Hz at room temperature. A unit cell (2032-type coin) was assembled by sandwiching the c-GPE between a Li metal anode and a liquid electrolyte (1 M $LiPF_6$ in EC/PC = 1/1 v/v)-soaked $LiCoO_2$ cathode. Assembly of cells was carried out in an argon-filled glove box. The charge/discharge behaviors of cells were examined with battery test equipment (PNE Solution). The discharge current densities varied from 0.2 C to 2.0 C at a constant charge current density of 0.2 C under a voltage range between 3.0 and 4.2 V. In addition, the cells were cycled at a constant charge/discharge current density of 0.5 C/0.5 C.

Fabrication of the Cu column arrays: On a piece of clean Si wafer, 5 nm Cr and 300 nm Cu were sputtered consecutively. The sputtered wafer was coated with photoresist AZ4620 at 2000 rpm for 30 s, and then was baked on hotplate at 110 °C for 2 min. A second layer of AZ4620 was coated with the same parameters, and then the wafer was baked on hotplate at 110 °C for 4 min. The final photoresist thickness was ~20 μm. Exposure was performed at a UV intensity of 3 mW/cm^2 for 90 s, followed by developing in solution of 1 part AZ400K and 2 parts DI water by volume. Different sized circles were opened up in the photoresist, to expose the Cu seed layer underneath. Electroplating of Cu column arrays was done in COPPER "P" BATH RTU (Technic incorporation) at 1 mA for 12 hours. After that, photoresist was removed by rinsing with acetone and isopropyl alcohol.

Supporting Information

Supporting Information is available from the Wiley Online Library or from the author.

Acknowledgements

This research was supported by Energy Efficiency and Resources R&D program (20112010100150) under the Ministry of Knowledge Economy, Republic of Korea. This work was also supported by the National Research Foundation of Korea Grant funded by the Korean Government (MEST) (NRF-2009-C1AAA001-2009-0093307).

Received: October 6, 2012
Revised: October 22, 2012
Published online: December 21, 2012

[1] a) M. Armand, J.-M. Tarascon, *Nature* **2008**, *451*, 652; b) B. Dunn, H. Kamath, J.-M. Tarascon, *Science* **2011**, *334*, 928; c) O. K. Park, Y. Cho, S. Lee, H.-C. Yoo, H.-K. Song, J. Cho, *Energy Environ. Sci.* **2011**, *4*, 1621.

[2] a) B. Scrosati, J. Garche, *J. Power Sources* **2010**, *195*, 2419; b) J.-M. Tarascon, M. Armand, *Nature* **2001**, *414*, 359; c) T. H. Hwang, Y. M. Lee, B.-S. Kong, J.-S. Seo, J. W. Choi, *Nano Lett.* **2012**, *12*, 802.

[3] a) L. Hu, H. Wu, F. L. Mantia, Y. Yang, Y. Cui, *ACS Nano* **2010**, *4*, 5843; b) A. M. Gaikwad, G. L. Whiting, D. A. Steingart, A. C. Arias, *Adv. Mater.* **2011**, *23*, 3251; c) J. F. M. Oudenhoven, L. Baggetto, P. H. L. Notten, *Adv. Energy. Mater.* **2011**, *1*, 10.

[4] H. Zhang, X. Yu, P. V. Braun, *Nat. Nanotechnol.* **2011**, *6*, 277.

[5] a) P. L. Taberna, S. Mitra, P. Poizot, P. Simon, J.-M. Tarascon, *Nature Mater.* **2006**, *5*, 567; b) M. M. Shaijumon, E. Perre, B. Daffos, P.-L. Taberna, J.-M. Tarascon, P. Simon, *Adv. Mater.,* **2010**, *22*, 4978.

[6] J. W. Long, B. Dunn, D. R. Rolison, H. S. White, *Chem. Rev.* **2004**, *104*, 4463.

[7] S. K. Cheah, E. Perre, M. Rooth, M. Fondell, A. Hårsta, L. Nyholm, M. Boman, T. Gustafsson, J. Lu, P. Simon, K. Edström, *Nano Lett.* **2009**, *9*, 3230.

[8] C. K. Chan, H. Peng, G. Liu, K. Mcilwrath, X. F. Zhang, R. A. Huggins, Y. Cui, *Nat. Nanotechnol.* **2008**, *3*, 31.

[9] S.-Y. Lee, W. H. Meyer, G. Wegner, *ChemPhysChem* **2005**, *6*, 49.

[10] J. Hassoun, S. Panero, P. Reale, B. Scrosati, *Adv. Mater.* **2009**, *21*, 4807.

[11] C. Gerbaldi, J. R. Nair, S. Ahmad, G. Meligrana, R. Bongiovanni, S. Bodoardo, N. Penazzi, *J. Power Sources* **2010**, *195*, 1706.

[12] M.-H. Ryou, Y. M. Lee, K. Y. Cho, G.-B. Han, J.-N. Lee, D. J. Lee, J. W. Choi, J.-K. Park, *Electrochim. Acta* **2012**, *60*, 23.

[13] E.-H. Kil, H.-J. Ha, S.-Y. Lee, *Macromol. Chem. Phys.* **2011**, *212*, 2217.

[14] H.-J. Ha, E.-H. Kil, Y. H. Kwon, J. Y. Kim, C. K. Lee, S.-Y. Lee, *Energy Environ. Sci.* **2012**, *5*, 6491.

[15] J. Yao, A.-P. Le, M. V. Schulmerich, J. Maria, T.-W. Lee, S. K. Gray, R. Bhargava, J. A. Rogers, R. G. Nuzzo, *ACS Nano,* **2011**, *5*, 5763.

[16] J. Park, J. H. Park, E. Kim, C. W. Ahn, H. I. Jang, J. A. Rogers, S. Jeon, *Adv. Mater.,* **2011**, *23*, 860.

[17] J. D. Ryckman, M. Liscidini, J. E. Sipe, S. M. Weiss, *Nano Lett.* **2011**, *11*, 1857.

[18] E. M. Benetti, C. Acikgoz, X. Sui, B. Vratzov, M. A. Hempenius, J. Huskens, G. J. Vancso, *Adv. Funct. Mater.* **2011**, *21*, 2088.

[19] T. Song, J. Xia, J.-H. Lee, D. H. Lee, M.-S. Kwon, J.-M. Choi, J. Wu, S. K. Doo, H. Chang, W. I. Park, D. S. Zang, H. Kim, Y. Huang, K.-C. Hwang, J. A. Rogers, U. Paik, *Nano Lett.,* **2010**, *10*, 1710.

[20] a) M. Ueno, N. Imanishi, K. Hanai, T. Kobayashi, A. Hirano, O. Yamamoto, Y. Takeda, *J. Power Sources* **2011**, *196*, 4756; b) R. Uchiyama, K. Kusagawa, K. Hanai, N. Imanishi, A. Hirano, Y. Takeda, *Solid State Ionics* **2009**, *180*, 205.

[21] G.-B. Han, M.-H. Ryou, K. Y. Cho, Y. M. Lee, J.-K. Park, *J. Power Sources* **2010**, *195*, 3709.

[22] a) S. Zhang, Z. Du, R. Lin, T. Jiang, G. Liu, X. Wu, D. Weng, *Adv. Mater.* **2010**, *22*, 5378; b) S. H. Nam, K. S. Kim, H.-S. Shim, S. H. Lee, G. Y. Jung, W. B. Kim, *Nano Lett.* **2011**, *11*, 3656.